

Fermi Large Area Telescope Observation of a Gamma-ray Source at the Position of Eta Carinae

A. A. Abdo^{1,2}, M. Ackermann³, M. Ajello³, A. Allafort³, L. Baldini⁴, J. Ballet⁵, G. Barbiellini^{6,7},
D. Bastieri^{8,9}, K. Bechtol³, R. Bellazzini⁴, B. Berenji³, R. D. Blandford³, E. Bonamente^{10,11},
A. W. Borgland³, A. Bouvier³, T. J. Brandt^{12,13}, J. Bregeon⁴, A. Brez⁴, M. Brigida^{14,15},
P. Bruel¹⁶, R. Buehler³, T. H. Burnett¹⁷, G. A. Caliendo¹⁸, R. A. Cameron³, P. A. Caraveo¹⁹,
S. Carrigan⁹, J. M. Casandjian⁵, C. Cecchi^{10,11}, Ö. Çelik^{20,21,22}, S. Chaty⁵, A. Chekhtman^{1,23},
C. C. Cheung^{1,2}, J. Chiang³, S. Ciprini¹¹, R. Claus³, J. Cohen-Tanugi²⁴, L. R. Cominsky²⁵,
J. Conrad^{26,27,28}, C. D. Dermer¹, F. de Palma^{14,15}, S. W. Digel³, E. do Couto e Silva³,
P. S. Drell³, R. Dubois³, D. Dumora^{29,30}, C. Favuzzi^{14,15}, S. J. Fegan¹⁶, E. C. Ferrara²⁰,
M. Frailis^{31,32}, Y. Fukazawa³³, P. Fusco^{14,15}, F. Gargano¹⁵, N. Gehrels²⁰, S. Germani^{10,11},
N. Giglietto^{14,15}, F. Giordano^{14,15}, G. Godfrey³, I. A. Grenier⁵, M.-H. Grondin^{29,30}, J. E. Grove¹,
L. Guillemot^{34,29,30}, S. Guiriec³⁵, D. Hadasch³⁶, Y. Hanabata³³, A. K. Harding²⁰, M. Hayashida³,
E. Hays²⁰, A. B. Hill^{37,38}, D. Horan¹⁶, R. E. Hughes¹³, R. Itoh³³, M. S. Jackson^{39,27},
G. Jóhannesson³, A. S. Johnson³, W. N. Johnson¹, T. Kamae³, H. Katagiri³³, J. Kataoka⁴⁰,
M. Kerr¹⁷, J. Knödseder¹², M. Kuss⁴, J. Lande³, L. Latronico⁴, S.-H. Lee³,
M. Lemoine-Goumard^{29,30}, M. Livingstone⁴¹, M. Llena Garde^{26,27}, F. Longo^{6,7}, F. Loparco^{14,15},
M. N. Lovellette¹, P. Lubrano^{10,11}, A. Makeev^{1,23}, M. N. Mazziotta¹⁵, J. E. McEnery^{20,42},
J. Mehault²⁴, P. F. Michelson³, W. Mitthumsiri³, T. Mizuno³³, A. A. Moiseev^{21,42}, C. Monte^{14,15},
M. E. Monzani³, A. Morselli⁴³, I. V. Moskalenko³, S. Murgia³, T. Nakamori⁴⁰,
M. Naumann-Godo⁵, P. L. Nolan³, J. P. Norris⁴⁴, E. Nuss²⁴, T. Ohsugi⁴⁵, A. Okumura⁴⁶,
N. Omodei³, E. Orlando⁴⁷, J. F. Ormes⁴⁴, M. Ozaki⁴⁶, J. H. Panetta³, D. Parent^{1,23}, V. Pelassa²⁴,
M. Pepe^{10,11}, M. Pesce-Rollins⁴, F. Piron²⁴, T. A. Porter³, S. Rainò^{14,15}, R. Rando^{8,9},
M. Razzano⁴, A. Reimer^{48,3}, O. Reimer^{48,3}, T. Reposeur^{29,30}, A. Y. Rodriguez¹⁸, R. W. Romani³,
M. Roth¹⁷, H. F.-W. Sadrozinski⁴⁹, A. Sander¹³, P. M. Saz Parkinson⁴⁹, J. D. Scargle⁵⁰, C. Sgrò⁴,
E. J. Siskind⁵¹, D. A. Smith^{29,30}, P. D. Smith¹³, G. Spandre⁴, P. Spinelli^{14,15}, M. S. Strickman¹,
D. J. Suson⁵², H. Takahashi⁴⁵, T. Takahashi⁴⁶, T. Tanaka³, J. B. Thayer³, J. G. Thayer³,
D. J. Thompson²⁰, L. Tibaldo^{8,9,5,53}, O. Tibolla⁵⁴, D. F. Torres^{18,36}, G. Tosti^{10,11},
A. Tramacere^{3,55,56}, Y. Uchiyama³, T. L. Usher³, J. Vandenbroucke³, V. Vasileiou^{21,22},
N. Vilchez¹², V. Vitale^{43,57}, A. P. Waite³, E. Wallace¹⁷, P. Wang³, B. L. Winer¹³, K. S. Wood¹,
Z. Yang^{26,27}, T. Ylinen^{39,58,27}, M. Ziegler⁴⁹

-
- ¹Space Science Division, Naval Research Laboratory, Washington, DC 20375, USA
- ²National Research Council Research Associate, National Academy of Sciences, Washington, DC 20001, USA
- ³W. W. Hansen Experimental Physics Laboratory, Kavli Institute for Particle Astrophysics and Cosmology, Department of Physics and SLAC National Accelerator Laboratory, Stanford University, Stanford, CA 94305, USA
- ⁴Istituto Nazionale di Fisica Nucleare, Sezione di Pisa, I-56127 Pisa, Italy
- ⁵Laboratoire AIM, CEA-IRFU/CNRS/Université Paris Diderot, Service d’Astrophysique, CEA Saclay, 91191 Gif sur Yvette, France
- ⁶Istituto Nazionale di Fisica Nucleare, Sezione di Trieste, I-34127 Trieste, Italy
- ⁷Dipartimento di Fisica, Università di Trieste, I-34127 Trieste, Italy
- ⁸Istituto Nazionale di Fisica Nucleare, Sezione di Padova, I-35131 Padova, Italy
- ⁹Dipartimento di Fisica “G. Galilei”, Università di Padova, I-35131 Padova, Italy
- ¹⁰Istituto Nazionale di Fisica Nucleare, Sezione di Perugia, I-06123 Perugia, Italy
- ¹¹Dipartimento di Fisica, Università degli Studi di Perugia, I-06123 Perugia, Italy
- ¹²Centre d’Étude Spatiale des Rayonnements, CNRS/UPS, BP 44346, F-30128 Toulouse Cedex 4, France, Jurgen.Knodseder@cesr.fr
- ¹³Department of Physics, Center for Cosmology and Astro-Particle Physics, The Ohio State University, Columbus, OH 43210, USA
- ¹⁴Dipartimento di Fisica “M. Merlin” dell’Università e del Politecnico di Bari, I-70126 Bari, Italy
- ¹⁵Istituto Nazionale di Fisica Nucleare, Sezione di Bari, 70126 Bari, Italy
- ¹⁶Laboratoire Leprince-Ringuet, École polytechnique, CNRS/IN2P3, Palaiseau, France
- ¹⁷Department of Physics, University of Washington, Seattle, WA 98195-1560, USA
- ¹⁸Institut de Ciències de l’Espai (IEEC-CSIC), Campus UAB, 08193 Barcelona, Spain
- ¹⁹INAF-Istituto di Astrofisica Spaziale e Fisica Cosmica, I-20133 Milano, Italy
- ²⁰NASA Goddard Space Flight Center, Greenbelt, MD 20771, USA
- ²¹Center for Research and Exploration in Space Science and Technology (CRESST) and NASA Goddard Space Flight Center, Greenbelt, MD 20771, USA
- ²²Department of Physics and Center for Space Sciences and Technology, University of Maryland Baltimore County, Baltimore, MD 21250, USA
- ²³George Mason University, Fairfax, VA 22030, USA
- ²⁴Laboratoire de Physique Théorique et Astroparticules, Université Montpellier 2, CNRS/IN2P3, Montpellier, France
- ²⁵Department of Physics and Astronomy, Sonoma State University, Rohnert Park, CA 94928-3609, USA
- ²⁶Department of Physics, Stockholm University, AlbaNova, SE-106 91 Stockholm, Sweden
- ²⁷The Oskar Klein Centre for Cosmoparticle Physics, AlbaNova, SE-106 91 Stockholm, Sweden
- ²⁸Royal Swedish Academy of Sciences Research Fellow, funded by a grant from the K. A. Wallenberg Foundation

-
- ²⁹CNRS/IN2P3, Centre d’Études Nucléaires Bordeaux Gradignan, UMR 5797, Gradignan, 33175, France
- ³⁰Université de Bordeaux, Centre d’Études Nucléaires Bordeaux Gradignan, UMR 5797, Gradignan, 33175, France
- ³¹Dipartimento di Fisica, Università di Udine and Istituto Nazionale di Fisica Nucleare, Sezione di Trieste, Gruppo Collegato di Udine, I-33100 Udine, Italy
- ³²Osservatorio Astronomico di Trieste, Istituto Nazionale di Astrofisica, I-34143 Trieste, Italy
- ³³Department of Physical Sciences, Hiroshima University, Higashi-Hiroshima, Hiroshima 739-8526, Japan
- ³⁴Max-Planck-Institut für Radioastronomie, Auf dem Hügel 69, 53121 Bonn, Germany
- ³⁵Center for Space Plasma and Aeronomic Research (CSPAR), University of Alabama in Huntsville, Huntsville, AL 35899, USA
- ³⁶Institució Catalana de Recerca i Estudis Avançats (ICREA), Barcelona, Spain
- ³⁷Université Joseph Fourier - Grenoble 1 / CNRS, laboratoire d’Astrophysique de Grenoble (LAOG) UMR 5571, BP 53, 38041 Grenoble Cedex 09, France
- ³⁸Funded by contract ERC-StG-200911 from the European Community
- ³⁹Department of Physics, Royal Institute of Technology (KTH), AlbaNova, SE-106 91 Stockholm, Sweden
- ⁴⁰Research Institute for Science and Engineering, Waseda University, 3-4-1, Okubo, Shinjuku, Tokyo, 169-8555 Japan
- ⁴¹Department of Physics, McGill University, Montreal, PQ, Canada H3A 2T8
- ⁴²Department of Physics and Department of Astronomy, University of Maryland, College Park, MD 20742, USA
- ⁴³Istituto Nazionale di Fisica Nucleare, Sezione di Roma “Tor Vergata”, I-00133 Roma, Italy
- ⁴⁴Department of Physics and Astronomy, University of Denver, Denver, CO 80208, USA
- ⁴⁵Hiroshima Astrophysical Science Center, Hiroshima University, Higashi-Hiroshima, Hiroshima 739-8526, Japan, hirotaka@hep01.hepl.hiroshima-u.ac.jp
- ⁴⁶Institute of Space and Astronautical Science, JAXA, 3-1-1 Yoshinodai, Sagami-hara, Kanagawa 229-8510, Japan
- ⁴⁷Max-Planck Institut für extraterrestrische Physik, 85748 Garching, Germany
- ⁴⁸Institut für Astro- und Teilchenphysik and Institut für Theoretische Physik, Leopold-Franzens-Universität Innsbruck, A-6020 Innsbruck, Austria
- ⁴⁹Santa Cruz Institute for Particle Physics, Department of Physics and Department of Astronomy and Astrophysics, University of California at Santa Cruz, Santa Cruz, CA 95064, USA
- ⁵⁰Space Sciences Division, NASA Ames Research Center, Moffett Field, CA 94035-1000, USA
- ⁵¹NYCB Real-Time Computing Inc., Lattingtown, NY 11560-1025, USA
- ⁵²Department of Chemistry and Physics, Purdue University Calumet, Hammond, IN 46323-2094, USA
- ⁵³Partially supported by the International Doctorate on Astroparticle Physics (IDAPP) program
- ⁵⁴Institut für Theoretische Physik and Astrophysik, Universität Würzburg, D-97074 Würzburg, Germany
- ⁵⁵Consorzio Interuniversitario per la Fisica Spaziale (CIFS), I-10133 Torino, Italy
- ⁵⁶INTEGRAL Science Data Centre, CH-1290 Versoix, Switzerland

ABSTRACT

The Large Area Telescope (LAT) onboard the *Fermi* Gamma-ray Space Telescope detected a γ -ray source that is spatially consistent with the location of Eta Carinae. This source has been persistently bright since the beginning of the LAT survey observations (from 2008 August to 2009 July, the time interval considered here). The γ -ray signal is detected significantly throughout the LAT energy band (i.e., up to ~ 100 GeV). The 0.1–100 GeV energy spectrum is well represented by a combination of a cutoff power-law model (< 10 GeV) and a hard power-law component (> 10 GeV). The total flux (> 100 MeV) is $3.7^{+0.3}_{-0.1} \times 10^{-7}$ photons $\text{s}^{-1} \text{cm}^{-2}$, with additional systematic uncertainties of 10%, and consistent with the average flux measured by *AGILE* (Tavani et al. 2009). The light curve obtained by *Fermi* is consistent with steady emission. Our observations do not confirm the presence of a γ -ray flare in 2008 October as reported by Tavani et al. (2009), although we cannot exclude that a flare lasting only a few hours escaped detection by the *Fermi* LAT. We also do not find any evidence for γ -ray variability that correlates with the large X-ray variability of Eta Carinae observed during 2008 December and 2009 January. We are thus not able to establish an unambiguous identification of the LAT source with Eta Carinae.

Subject headings: stars: binaries: general — stars: supergiants — stars: individual (Eta Carinae)

1. Introduction

Eta Carinae (hereafter η Car), with its famous bipolar nebula, is in the Carina nebula at a distance of 2.3 kpc (Davidson & Humphreys 1997). The star is a luminous blue variable which is thought to be near the onset of pulsational instabilities. Since the flux from radio to X-ray is known to vary with a period of 5.54 yr (Damineli et al. 2008), η Car is considered to have a companion star and hence be in a binary system. Around periastron, the 2–10 keV X-ray light curve first increases gradually and then drops sharply to the minimum by more than one order of magnitude (Hamaguchi et al. 2007). After the faintest state lasting a few months, the source returns to the nominal flux. The last periastron passage was in 2008 December – 2009 January and the X-ray flux behaved in a similar fashion as observed in previous orbits (Corcoran 2009).

The binary system parameters of η Car are currently estimated as follows: stellar masses $M_\eta \sim 120M_\odot$ and $M_c \sim 30M_\odot$ with an eccentricity of 0.9–0.95, mass-loss rates and terminal velocities of the stellar winds $\dot{M}_\eta \sim 10^{-4}M_\odot \text{yr}^{-1}$, $\dot{M}_c \sim 10^{-5}M_\odot \text{yr}^{-1}$, $v_{\eta,\infty} \sim 500 \text{ km s}^{-1}$

⁵⁷Dipartimento di Fisica, Università di Roma “Tor Vergata”, I-00133 Roma, Italy

⁵⁸School of Pure and Applied Natural Sciences, University of Kalmar, SE-391 82 Kalmar, Sweden

and $v_{c,\infty} \sim 3000 \text{ km s}^{-1}$, where the subscripts η and c represent η Car and the companion, respectively (Kashi & Soker 2009, where references are given). Such binary systems with stellar winds at high mass-loss rates and velocities are called colliding wind binaries (CWBs), and are theoretically predicted to be potential sites of high-energy γ -ray emission through strong shocks due to the colliding winds (Eichler & Usov 1993), although there have been no distinct observational detections of γ -rays from CWBs so far.

Recently, two γ -ray satellites, *AGILE* and *Fermi* discovered a γ -ray source that is spatially consistent with η Car (Tavani et al. 2009; Abdo et al. 2009a). The source also overlaps with the error circles of the unidentified COS-B and EGRET sources, 2CG 288–00 (Swanenburg et al. 1981) and 3EG J1048–584 (Hartman et al. 1999). If this source were indeed associated with η Car, it would be the first time that a CWB is observed in high-energy γ -rays. Tavani et al. (2009) reported the γ -ray average flux ($> 100 \text{ MeV}$) of $3.7 \pm 0.5 \times 10^{-7} \text{ photons s}^{-1} \text{ cm}^{-2}$ and an increase of γ -ray flux 5–9 times above the average on a time scale of 2 days in 2008 October. In this letter, we analyze the γ -ray source observed by the Large Area Telescope (LAT) onboard *Fermi* covering the recent periastron passage, and discuss the possibility of the association with η Car. Hereafter, we refer to the γ -ray source as 1FGL J1045.2–5942 as quoted in the *Fermi* LAT first source catalog (Abdo et al. 2010b).

2. Data Reduction and Results

The *Fermi* Gamma-ray Space Telescope was launched on 2008 June 11th and the LAT instrument began nominal sky-survey observations on 2008 August 4th. In this survey mode, the LAT scans the sky completely every 2 orbits (~ 3 hours); details of the LAT performance are described in Atwood et al. (2009). To study the γ -ray spectrum and light curve of 1FGL J1045.2–5942, here we analyze the LAT data observed from 2008 August 4th to 2009 July 23rd, with the standard analysis software of Science Tools version v9r11 and the instrument response function of P6_V3_DIFFUSE. To minimize background, we used only the “diffuse” class events (events which have the highest probability of being photons), and require the reconstructed zenith angles to be less than 105° in order to exclude Earth’s albedo photons. Within the radius of 10° around 1FGL J1045.2–5942, there are no γ -ray bursts detected by the LAT during this exposure. The systematic uncertainty of the effective area of the response function (P6_V3_DIFFUSE) is estimated to be 10%, 5% and 20% at 100 MeV, 560 MeV and 10 GeV, respectively. In the following analysis, we also consider the γ -ray emission from the pulsars PSR J1048–5832 and PSR J1028–5819 [see Abdo et al. (2009b; 2009e) for details of these pulsars] as a comparison. These pulsars are only $\sim 1^\circ$ and $\sim 2.5^\circ$ away from 1FGL J1045.2–5942 and like most pulsars, display no significant variability (except for their pulsations). The comparison of the light curves and spectra for the three sources provides an estimate of their relative variabilities or differences, regardless of systematic uncertainties.

Figure 1 shows counts maps around 1FGL J1045.2–5942 for the energy bands of 0.1–10 GeV and 10–100 GeV. In addition to the bright pulsars PSR J1048–5832 and PSR J1028–5819 in the

soft energy band, 1FGL J1045.2–5942 is clearly detected in both soft and hard energy bands and is the brightest γ -ray source above 10 GeV in this region. Applying the source-finding tool (`gtfindsrc`) for the total 0.1–100 GeV band, the position (J2000) of 1FGL J1045.2–5942 is obtained as $(\alpha, \delta) = (161.281, -59.710)$ with the 95% statistic error of $0^\circ.025$. This result is consistent with the *Fermi* LAT first source catalog (Abdo et al. 2010b), and places η Car slightly outside the 95% error region (offset $0^\circ.03$). However, when we perform the same analyses for the soft and hard bands separately, the source position is estimated as $(\alpha, \delta) = (161.312, -59.713)$ with the 95% error of $0^\circ.062$ and $(161.265, -59.695)$ with the error of $0^\circ.031$, respectively. The hard band position is offset by only $0^\circ.01$ from the location of η Car and thus is fully consistent with the object. The soft band position is offset by $0^\circ.04$ from η Car, yet due to the larger uncertainty in the soft band we cannot conclude whether the LAT indeed detects two distinct sources or whether the soft and hard components arise from the same object. On the other hand, despite the many interesting nearby sources [the hard X-ray source IGR J10447–6027 and the anomalous X-ray pulsar 1E 1048.1–5937 that have been detected by *INTEGRAL* (Leyder et al. 2008) and other bright X-ray sources (WR 25, HD 93129A/B, HD 93250, HD 93205 and HD 93160) as well as the recently-discovered neutron star (Hamaguchi et al. 2009)], none of these fall in the 95% LAT error circle.

2.1. Spectral Analysis

To measure the time-averaged energy spectrum of 1FGL J1045.2–5942, we performed a spectral analysis with the maximum likelihood fitting tool (`gtlike`). We selected a region of interest (ROI) with radius of 10° around the source and modeled the observed γ -ray emission with a combination of point sources, Galactic and extragalactic diffuse emission, and residual instrumental background. Within the ROI, we found 25 point-like sources of which 4 have been identified as pulsars (Abdo et al. 2010b). We modeled the spectra of the pulsars using an exponentially cut-off power-law (CPL) model, $E^{-\Gamma} \exp(-E/E_{\text{cutoff}})$, while the other sources are modeled using a simple power-law (PL) model, $E^{-\Gamma}$, where E is the photon energy, Γ is the photon index and E_{cutoff} is the cutoff energy. The Galactic diffuse emission was modeled using GALPROP (e.g., Strong & Moskalenko 1998), version “gll_iem_v01.fit”, and the extragalactic diffuse emission and residual instrumental backgrounds were combined into a spatially uniform component with a power-law spectral model.¹

The resulting 0.1–100 GeV spectra of 1FGL J1045.2–5942 and PSR J1048–5832 are shown in Figure 2 (a). The integrated photon flux (> 100 MeV) and spectral parameters of PSR J1048–5832 are obtained as $F(> 100\text{MeV}) = 2.6^{+0.3}_{-0.4} \times 10^{-7}$ photons $\text{s}^{-1} \text{cm}^{-2}$, $\Gamma = 1.4 \pm 0.2$ and $E_{\text{cutoff}} = 2.0^{+0.6}_{-0.4}$ GeV with additional systematic uncertainties of $\sim 10\%$, and consistent with the values obtained by Abdo et al. (2009b). Compared with the good CPL fit of PSR J1048–5832, the spectrum of 1FGL

¹A check with the more-recent LAT-team model for diffuse emission, gll_iem_v02.fit, and isotropic spectrum isotropic_iem_v02.txt yielded entirely consistent results.

J1045.2–5942 has a similar convex shape below 10 GeV, but shows a hard emission tail above 10 GeV. The 10–100 GeV emission of 1FGL J1045.2–5942 is detected at a significance level of $> 11\sigma$ (and 6σ even including the systematic uncertainty), while for PSR J1048–5832 only upper limits are obtained above 10 GeV. This result is consistent with that in Figure 1, where 1FGL J1045.2–5942 is clearly brighter than PSR J1048–5832 in the > 10 GeV map. Therefore, the 100 MeV–100 GeV spectrum cannot be fitted by either the single PL or CPL model, and is represented well by their combination (CPL+PL model). As the obtained physical parameters are summarized in Table 1, the log likelihood (L) differences of $-2 \times \Delta \log(L)$, corresponding to the test statistic (TS) value, for a single CPL and the CPL+PL model with respect to the single PL are 4 and 68, respectively. From the CPL+PL model, we obtain $\Gamma = 1.6 \pm 0.2$ and $E_{\text{cutoff}} = 1.6^{+0.8}_{-0.5}$ GeV for the low-energy CPL model, and $\Gamma = 1.9^{+0.2}_{-0.3}$ for the high-energy PL component. The fluxes below/above 10 GeV are measured as $F(0.1\text{--}10 \text{ GeV}) = 3.7^{+0.3}_{-0.1} \times 10^{-7} \text{ photons s}^{-1} \text{ cm}^{-2}$ and $F(> 10 \text{ GeV}) = (8 \pm 2) \times 10^{-10} \text{ photons s}^{-1} \text{ cm}^{-2}$, and the total energy flux (0.1–100 GeV) is obtained as $(2.4 \pm 0.1) \times 10^{-10} + (0.4 \pm 0.1) \times 10^{-10} = (2.8 \pm 0.2) \times 10^{-10} \text{ ergs s}^{-1} \text{ cm}^{-2}$, where the systematic uncertainties are $\sim 10\%$ and 20% below and above 10 GeV, respectively. Therefore, the obtained photon flux (> 100 MeV) by the *Fermi* LAT is consistent with that reported by *AGILE* (Tavani et al. 2009).

There is one unidentified EGRET source, 3EG J1048–5840 (α, δ) = (162.14, -58.68) with the 95% error circle of $0^\circ.17$ (Hartman et al. 1999), close to the positions of 1FGL J1045.2–5942 and PSR J1048–5832, as shown in Figure 1. The summed flux of 1FGL J1045.2–5942 and PSR J1048–5832 is $\sim 6.3 \times 10^{-7} \text{ photons s}^{-1} \text{ cm}^{-2}$, and is consistent with that of 3EG J1048–5840 [$(6.2 \pm 0.7) \times 10^{-7} \text{ photons s}^{-1} \text{ cm}^{-2}$]. Therefore, it is plausible that the EGRET source was the sum of the two LAT sources (see also Abdo et al. 2009b).

In Figure 2 (b) we compare the high-energy γ -ray spectrum of 1FGL J1045.2–5942 to X-ray spectra of η Car. The X-ray telescope (XRT) onboard the *Swift* satellite (Burrows et al. 2005) observed η Car every 2 days during the last periastron passage, where the X-ray flux below 10 keV decreased continuously more than one order of magnitude. We analyzed the archival clean data in the standard way and show two 0.5–10 keV spectra of the first observation on 2008 December 19–20 (the highest flux; obsid 00031308002) and the last observation on 2009 January 14 (the lowest flux; obsid 00031308009) as the representatives. There are prominent Fe-K α lines at 6–7 keV coming from the optically-thin thermal plasma, and the spectral shape as well as the variability is similar to that observed in the periastron passage (Hamaguchi et al. 2007). Above 10 keV, there are three observations by the *INTEGRAL* and *Suzaku* satellites to report detection of the X-ray hard tail from η Car up to 50–100 keV almost free of contamination from surrounding sources (Leyder et al. 2008; Sekiguchi et al. 2009). We also plot the flux of the hard tail emission which is represented by a single PL model without the contribution of the soft thermal emission dominated below 10 keV. Although the observations were performed before the launch of the *Fermi* satellite and not simultaneous and the variation of the hard X-ray emission is still uncertain along the orbit, the γ -ray spectrum of 1FGL J1045.2–5942 is smoothly connected to the X-ray spectra of η Car with the

photon index of ~ 2 , which is consistent with theoretical prediction of inverse-Compton emission from the CWB system (e.g., Reimer et al. 2006).

2.2. Timing Analysis

X-ray observations have detected intense variability from η Car in 2008–2009 (Corcoran 2009), and Tavani et al. (2009) also reported a large γ -ray flare on 2008 October 11–13 on a time scale of 2 days by *AGILE*. To study the association between the γ -ray source and η Car, it is very important to search for coincident variability in their light curves. Therefore, we generated the 0.1–100 GeV light curve of 1FGL J1045.2–5942 from the 1-year LAT dataset by aperture photometry with an aperture of $0^\circ.5$ (using *gtbin* and *gtexposure* tools). We perform this analysis on a time scale of 2 days to compare with the result of Tavani et al. (2009) who used the same time scale.

Figure 3 shows the resulting 2-day light curve, where the contribution of the Galactic and extragalactic diffuse emission within this aperture of 3.2×10^{-7} photons $\text{s}^{-1} \text{cm}^{-2}$ that is obtained from the spectral analysis is subtracted. Our light curve does not show any evidence for flaring activity on a 2-day time scale. The deviation from constant flux is $\chi^2/dof = 169/175 \sim 1$ and can be fully attributed to statistical fluctuations. The largest 2-day flux amounts to $(9 \pm 3) \times 10^{-7}$ photons $\text{s}^{-1} \text{cm}^{-2}$ which present a $\sim 2\sigma$ deviation from the average value of 3.7×10^{-7} photons $\text{s}^{-1} \text{cm}^{-2}$. Although the average flux is consistent with that obtained by *AGILE* as mentioned in § 2.1, we do not detect the large γ -ray flare of $(27.0 \pm 6.5) \times 10^{-7}$ photons $\text{s}^{-1} \text{cm}^{-2}$ (6–10 times brighter than the average) that has been reported by Tavani et al. (2009), which if it existed, should have been easily detected by the *Fermi* LAT.

To compare the LAT data with the *AGILE* results more directly, Figure 4 shows the counts maps around 1FGL J1045.2–5942 with the same 2-day binning as Fig. 2 of Tavani et al. (2009), where the LAT map labeled “Oct 11–13” covers the epoch of the large flare by *AGILE* (i.e., from 2008 October 11th 02:27 to 13th 04:16 UT). As shown in Figure 1, the average flux at PSR J1028–5819 is the highest in this region ($\sim 30\%$ brighter than that at 1FGL J1045.2–5942). This trend is also the same for all the four 2-day maps and is consistent with the result obtained in the above light curve, although there are statistical fluctuations due to the limited number of detected events in the short exposure.

Because the *AGILE* satellite provides good sensitivity to ~ 100 MeV γ -rays, the flare reported by Tavani et al. (2009) may only have occurred at low energies where the LAT effective area drops rapidly with the “diffuse” event selection that was used in this work (Atwood et al. 2009). We therefore also perform a light curve analysis in the 100–400 MeV energy band, for which we employ a 2° extraction radius to take into account the increase in size of the point spread function at lower energies. Table 2 summarizes the number of events detected around the position of 1FGL J1045.2–5942 by the LAT in each period. In addition to photons from 1FGL J1045.2–5942, those events include photons from diffuse Galactic and extragalactic emission and the two nearby pulsars

PSR J1048–5832 and PSR J1028–5819. We calculate that the mean number of events from 1FGL J1045.2–5942 in each time period is ~ 6 counts ($\sim 1/7$ of the total) and ~ 5 counts ($\sim 1/2$ of the total) for the 100–400 MeV band within 2° and 0.1–100 GeV within 0.5° , respectively. These numbers are statistically consistent among the four periods, and we conclude that the flux of 1FGL J1045.2–5942 does not vary significantly over the entire week in not only the total 0.1–100 GeV band but also the softer 100–400 MeV band. If the large flare reported by Tavani et al. (2009) occurred within the field of view of the LAT and the flux of 1FGL J1045.2–5942 increased by 6–10 times higher than the average in only the soft energy band around 100 MeV, the total number of the events detected by the LAT in 100–400 MeV should have increased by ~ 35 –60 counts (a factor of 2–3), which corresponds to the 5 – 9σ increase. Again we conclude that this should have been easily detected by the *Fermi* LAT.

In Figure 5 we plot the LAT effective area within the radius of 2° around 1FGL J1045.2–5942 in 0.1–100 GeV and 100–400 MeV obtained by `gtexposure` around the time of the *AGILE* large flare, as well as the off-axis angle from the LAT boresight to the source. The tool `gtexposure` calculates the spectrally-weighted average exposure (in the unit of “cm² s”) also taking into account the truncation of the point spread function by the finite size of the aperture toward the source region. To obtain the effective area (“cm²”) for both 0.1–100 GeV and 100–400 MeV bands, we performed `gtexposure` assuming the photon index of 2.0 with the time binning of 60 s and the 2° radius, and divided the output by 60 s. The absolute value of the 100–400 MeV area is about half of that of the total 0.1–100 GeV band, and large enough to detect the flare as described above with the actual number of the detected events. Since *Fermi* was operating in survey mode, 1FGL J1045.2–5942 was observed in a repeating pattern every two orbits (~ 3 hours), with a duration of ~ 50 minutes in the first orbit at boresight angles between 0° and 70° (= the size of the LAT field of view), and with a duration of ~ 20 minutes in the second orbit at the boresight angle only around 70° . The LAT observed the source near the edge of the field of view in the second orbit, and the effective area toward the source was not very efficient during the time. Therefore, we note that the time coverage of η Car by both satellites is not identical, and the large flare reported by *AGILE* could have escaped detection by the *Fermi* LAT if it lasted for only a few hours. However, restricting the *AGILE* detected flare duration to ~ 2 hours would imply that the source flux increased by approximately 120–220 times the average.

To search for γ -ray variability coincident with the X-ray variability of η Car, which occurs on time scales of a few months, we also obtained the LAT light curves with 1-week binning for 1FGL J1045.2–5942, and for comparison also PSR J1048–5832 and PSR J1028–5819. We analyzed the 0.1–10 GeV events during every 7 days by the same likelihood method described in § 2.1, but fixing the photon index and cutoff energy (i.e., spectral shape) of each source at its average values and keeping only the flux as a free parameter. For all 1FGL J1045.2–5942, PSR J1048–5832 and PSR J1028–5819, the CPL model was used. This method, fitting all the detected events within the ROI of 10° , models the contamination from other sources and the diffuse background, and measures the fluxes of all the three sources simultaneously. In each week, 1FGL J1045.2–5942 is detected with a

TS value of at least 10 (typically ~ 40), and the resulting light curves are shown in Figure 6 as well as the 2–10 keV X-ray light curve of η Car (Corcoran 2009) obtained by the Proportional Counter Array (PCA) onboard *Rossi X-ray Timing Explorer* (Jahoda et al. 1996). The deviations of the γ -ray light curves from the constant fluxes are $\chi^2/dof = 43/50$ (the probability to be consistent with the mean is $P = 75\%$) for 1FGL J1045.2–5942, $41/50$ ($P = 81\%$) for PSR J1048–5832 and $53/50$ for PSR J1028–5819 ($P = 36\%$), where we applied 3% systematic uncertainty derived in the Fermi LAT first source catalog (Abdo et al. 2010b). Since PSR J1048–5832 and PSR J1028–5819 are thought to be stable sources and there is no significant deviation in their light curves. We conclude that 1FGL J1045.2–5942 does not show any significant variability on the time scale of > 1 week, either. Above 10 GeV, the number of events detected from 1FGL J1045.2–5942 integrated over the current 1-year observation amounts to only ~ 30 , which makes a variability analysis in this band unfeasible.

Subtracting the contamination from surrounding sources in the *RXTE* PCA field of view, the optically-thin thermal X-ray emission below 10 keV from η Car itself varies by \sim two orders of magnitude around the periastron passage (Figure 2 and Hamaguchi et al. 2007). In contrast, the obtained γ -ray light curve of 1FGL J1045.2–5942 is rather steady even during the last periastron passage of η Car in 2009 January (Figure 6), with the possible fluctuation of at most $\pm 2 \times 10^{-7}$ photons $\text{s}^{-1} \text{cm}^{-2}$ or a factor of ~ 3 .

To investigate the possible variation of 1FGL J1045.2–5942 coincident with the X-ray light curve of η Car, we next accumulated the LAT events into three periods to increase the statistics. Referring to the X-ray light curve of η Car, the γ -ray data are divided as shown in Figure 6; the X-ray flux of η Car increased in Period 1, decreased by more than an order of magnitude in Period 2 and returned to the average in Period 3. From the 0.1–10 GeV likelihood analysis of each period in the same way as that in § 2.1 (i.e., all the spectral parameters are fitted freely), the γ -ray source 1FGL J1045.2–5942 was detected significantly in each period with TS values of 750, 231 and 830, respectively. Their spectra and the obtained parameters are shown in Figure 7 and Table 3, respectively. We also performed the same 0.1–10 GeV analysis for the average data and determined the spectral shape as shown in Figure 2 (a), to compare the results one another including the average spectrum. The power-law index and cutoff energy in all the periods are consistent with the values determined for the total dataset. This result confirms that 1FGL J1045.2–5942 is detected close to the average flux even during the X-ray faintest state of η Car (Period 2), and the γ -ray variability (if it exists) is very small (at most a factor of ~ 1.5) compared with that in X-ray ($>$ one order of magnitude).

The similarity of the spectra of 1FGL J1045.2–5942 and PSR J1048–5832 below 10 GeV may suggest that 1FGL J1045.2–5942 could be associated with a yet unknown pulsar. However, using our 1-year dataset, we searched for possible pulsations by the blind search technique (Atwood et al. 2006) like other LAT pulsars, and did not detect any pulsations on time scales from several tens of milliseconds to 1 day. Considering the number of events detected from 1FGL J1045.2–5942 is ~ 5000 , the upper limit of the pulsed flux is estimated as $\sim 10\%$ level of the 1FGL J1045.2–5942

flux, i.e., as $\sim 3 \times 10^{-8}$ photons $\text{s}^{-1} \text{cm}^{-2}$.

Given the pulsar-like spectrum of 1FGL J1045.2–5942, we also searched for X-ray pulsations in an archival *RXTE* observation of the Anomalous X-ray Pulsar 1E 1048.1–5937 with 1FGL J1045.2–5942 in the 1° field of view (Jahoda et al. 2006). We chose an observation from 1996 September 29–30, spanning 99 ks with 53 ks of exposure (Obsid 10192-03), and selected events from the top Xenon detection layer, from all 5 Proportional Counter Units (PCUs), in the energy range ~ 2 –10 keV. After each photon was barycentered using the position of 1FGL J1045.2–5942, time series were created with 1/512 s time resolution. We then performed a Fast Fourier Transform and searched for a peak in the power spectrum not harmonically related to the bright Anomalous X-ray Pulsar ($P=6.452$ s). As a result, we found no evidence for a pulsed signal in the X-ray band, either. According to the time resolution of the time series and strong red noise in the power spectrum, the obtained result is sensitive to pulsations with frequencies between 10 ms and 100 s. Following the methods in van der Klis (1989) and Vaughan et al. (1994), the 99% confidence upper limit on a sinusoidal pulsed signal is estimated to be $0.14 \text{ count s}^{-1} \text{PCU}^{-1}$ corresponding to $3.1 \times 10^{-13} \text{ ergs s}^{-1} \text{cm}^{-2}$ (2–10 keV), where a simple power-law model with a spectral index of 2.0 and an absorption column density of $1 \times 10^{21} \text{ cm}^{-2}$ are assumed.

3. Discussion

Our analysis of the 1st year *Fermi* LAT dataset revealed a γ -ray source (1FGL J1045.2–5942) that is spatially consistent with the location of η Car. The average flux (> 100 MeV) is measured as $3.7_{-0.1}^{+0.3} \times 10^{-7}$ photons $\text{s}^{-1} \text{cm}^{-2}$, and consistent with that reported by *AGILE* (Tavani et al. 2009). The γ -ray signal is detected significantly throughout the LAT energy band up to ~ 100 GeV. The 0.1–100 GeV energy spectrum cannot be fit by either a single PL or CPL model, but is represented well by a combination of a cutoff power-law model (< 10 GeV) and a hard power-law component (> 10 GeV). As one of the most powerful colliding wind binary systems that is known, η Car is certainly a promising candidate for the underlying source of 1FGL J1045.2–5942. Although the hard X-ray observations were not performed simultaneously with *Fermi*, the measured γ -ray spectrum is smoothly connected to the hard X-ray emission above 10 keV from η Car with the photon index of ~ 2 , which is consistent with the theoretical study of CWBs, namely the spectrum from the inverse-Compton emission by the interaction between stellar photons and accelerated particles at the colliding-wind regions (e.g., Reimer et al. 2006), yet so far we have no convincing evidence (such as correlated time variability or flaring events) that allows a physical link to be established. In particular, our 2-day light curve does not show any indication for short duration γ -ray flares in either softer 100–400 MeV or total 0.1–100 GeV bands and we are unable to confirm the large γ -ray flare on 2008 October 11–13 reported by Tavani et al. (2009).

As blazars are the dominant source population of the GeV sky, we cannot exclude the possibility that 1FGL J1045.2–5942 is associated with a background blazar in the direction of the Carina nebula. Three arguments, however, disfavor such an hypothesis. Firstly, the probability of finding

at least one background blazar within the 95% confidence region of 1FGL J1045.2–5942 amounts to only 7×10^{-5} (Abdo et al. 2010b). We estimate this probability from the source density of ~ 90 high-latitude GeV sources per sr (which mostly are blazars) with 1–100 GeV fluxes of $\gtrsim 1 \times 10^{-9}$ photons $\text{s}^{-1} \text{cm}^{-2}$ and from the solid angle of about 8×10^{-7} sr of the 95% confidence error region. Secondly, 1FGL J1045.2–5942 appears to be a stable source in contrast to many blazars that are time variable (Abdo et al. 2009c). Thirdly, the spectrum of 1FGL J1045.2–5942 is rather complex, combining an exponentially cut-off power-law spectrum with an additional hard power-law tail at high energies. None of the blazars observed by *Fermi* shows similar spectral characteristics.

On the other hand, the spectrum is qualitatively very similar to that observed from the Crab (Abdo et al. 2010a). While for the Crab, the exponentially cutoff power-law is attributed to the pulsar, the high-energy power-law component is attributed to the pulsar wind nebula. Since the LAT has recently discovered many γ -ray bright but radio and X-ray faint or quiet pulsars (Abdo et al. 2009d), a pulsar and its nebula may represent a reasonable explanation for the observed emission, although no pulsar or pulsar wind nebula is yet known near η Car. However, η Car is a member of the young and massive open star cluster Tr 16 that may well house some young and energetic pulsars, similar to PSR J2032+4127 which has been recently discovered by the *Fermi* LAT toward the Cyg OB2 massive star cluster (Abdo et al. 2009d; Camilo et al. 2009), and may be associated with the unidentified TeV source TeV J2032+4130 (Aharonian et al. 2005) that may represent the corresponding pulsar wind nebula. Alternatively, the exponentially cutoff power-law and the hard power-law components could arise from two physically unassociated sources, although the positions obtained in the < 10 GeV and > 10 GeV bands are close enough to be consistent within the current statistical uncertainty.

In any case, the study of the variability of 1FGL J1045.2–5942 will be key to identify the underlying source. Were 1FGL J1045.2–5942 to be related to η Car, some modulation of the γ -ray flux is expected during the 5.54 yr long orbit (Reimer et al. 2006) and the *Fermi* LAT is ideally suited to reveal this modulation. On the other hand, were 1FGL J1045.2–5942 a pulsar, the pulsation might be detected below the current upper limits in γ -ray and X-ray, and help may also come from a deep radio search that is able to unveil young and energetic pulsars. Furthermore, deep observations in the TeV domain by *HESS* and *CANGAROO*, and in the future *CTA* may reveal the related pulsar wind nebula if it exists.

The *Fermi* LAT Collaboration acknowledges support from a number of agencies and institutes for both development and the operation of the LAT as well as scientific data analysis. These include NASA and DOE in the United States, CEA/Irfu and IN2P3/CNRS in France, ASI and INFN in Italy, MEXT, KEK, and JAXA in Japan, and the K. A. Wallenberg Foundation, the Swedish Research Council and the National Space Board in Sweden. Additional support from INAF in Italy and CNES in France for science analysis during the operations phase is also gratefully acknowledged. We thank M. Corcoran for providing the X-ray light curve of η Car by the *RXTE* PCA in Figure 3.

Facilities: Fermi (LAT).

REFERENCES

- Abdo, A. A., et al., 2008, *Science*, 322, 1218
- Abdo A. A., et al., 2009a (LAT bright source list), *ApJS*, 183, 46
- Abdo A. A., et al., 2009b (PSR J1048–5832 and PSR J2229+6114), *ApJ*, 706, 1331
- Abdo, A. A., et al., 2009c (LAT AGN source list), *ApJ*, 700, 597
- Abdo, A. A., et al., 2009d (16 Pulsars), *Science*, 325, 840
- Abdo, A. A., et al., 2009e (PSR J1028–5819), *ApJ*, 695, 72
- Abdo, A. A., et al., 2010a (Crab), *ApJ*, 708, 1254
- Abdo, A. A., et al., 2010b (LAT first-year source list), in preparation,
http://fermi.gsfc.nasa.gov/ssc/data/access/lat/1yr_catalog/
- Aharonian, F., et al., 2005, *Å*, 431, 197
- Atwood, W. B., et al., 2009, *ApJ*, 697, 1071
- Atwood, W. B., Ziegler, M., Johnson, R. P., & Baughman, B., M., 2006, *ApJ*, 652, L49
- Burrows, D. N., et al., 2005, *Space Science Reviews*, 120, 165
- Camilo, F., et al., 2009, *ApJ*, 705, 1
- Corcoran, M., http://asd.gsfc.nasa.gov/Michael.Corcoran/eta_car/etacar_rxte_lightcurve/index.htm
- Damineli, A., et al., 2008, *MNRAS*, 384, 1649
- Davidson, K., & Humphreys, R. M., 1997, *ARA&A*, 35, 1
- Eichler, D., & Usov, V., 1993, *ApJ*, 402, 271
- Hamaguchi, K., et al., 2007, *ApJ*, 663, 522
- Hamaguchi, K., et al., 2009, *ApJ*, 695, 4
- Hartman, R. C., et al., 1999, *ApJS*, 123, 79
- Jahoda, K., Markwardt, C. B., Radeva, Y., Rots, A. H., Stark, M. J., Swank, J. H., Strohmayer, T. E., & Zhang, W., 2006, *ApJS*, 163, 401

- Jahoda, K., Swank, J. H., Giles, A. B., Stark, M. J., Strohmayer, T., Zhang, W., & Morgan, E. H., 1996, SPIE, 2808, 59
- Kashi, A., & Soker, N., 2009, New A, 14, 11
- Leyder, J.-C., Walter, R., & Rauw, G., 2008, *A&A*, 477, L29
- Reimer, A., Pohl, M., & Reimer, O., 2006, ApJ, 644, 1118
- Sekiguchi, A., Tsujimoto, M., Kitamoto, S., Ishida, M., Hamaguchi, K., Mori, H., & Tsuboi, Y., 2009, PASJ, 61, 629
- Strong, A. W., & Moskalenko, I. V., 1998, ApJ, 509, 212
- Swanenburg, B. N., et al., 1981, ApJ, 243, 69
- Tavani, M., et al., 2009, ApJ, 698, 142
- van der Klis, M., 1989, Timing Neutron Stars, 27
- Vaughan, B. A., et al., 1994, ApJ, 435, 362

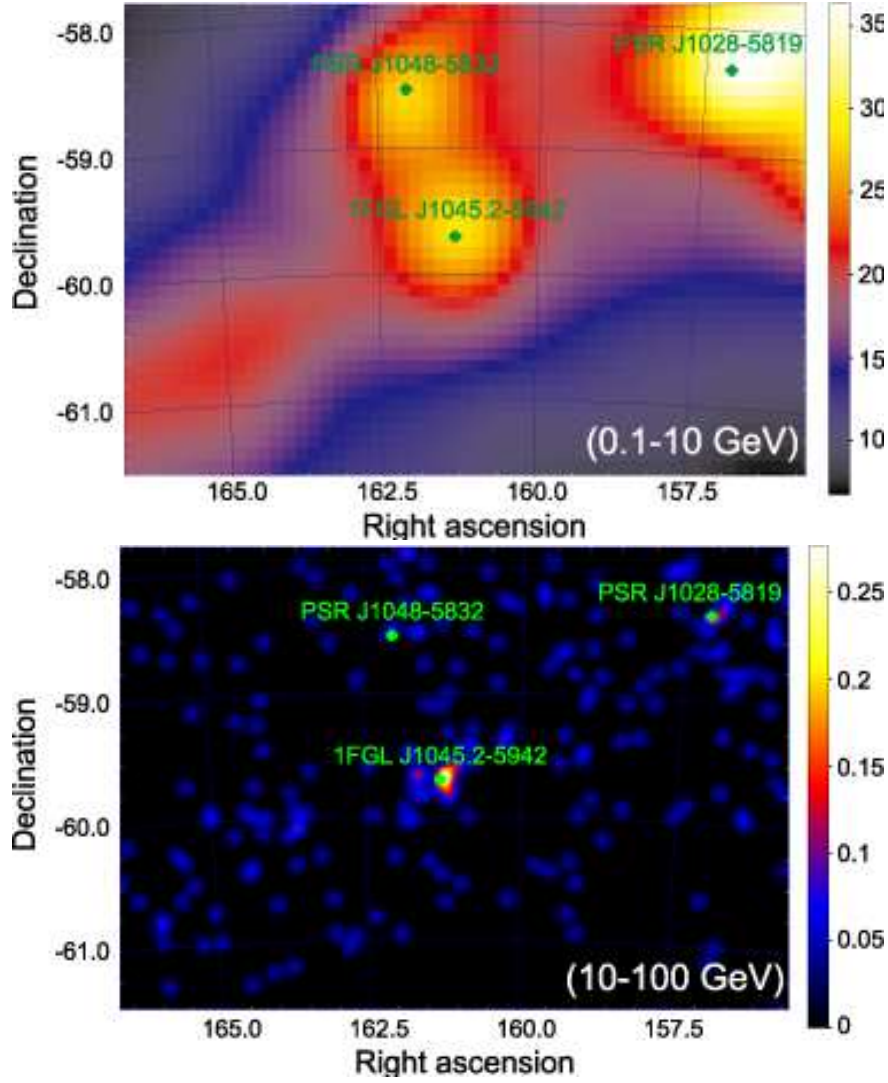


Fig. 1.— Counts maps around 1FGL J1045.2–5942 with the energy bands of 0.1–10 GeV (top) and 10–100 GeV (bottom), where the pixel sizes are $0''.1$ with 6-bin Gaussian smoothing and $0''.025$ with 4-bin smoothing, respectively. The unit of the color bars is counts pixel $^{-2}$. Green crosses indicate the positions of the *Fermi* LAT first source catalog (Abdo et al. 2010b).

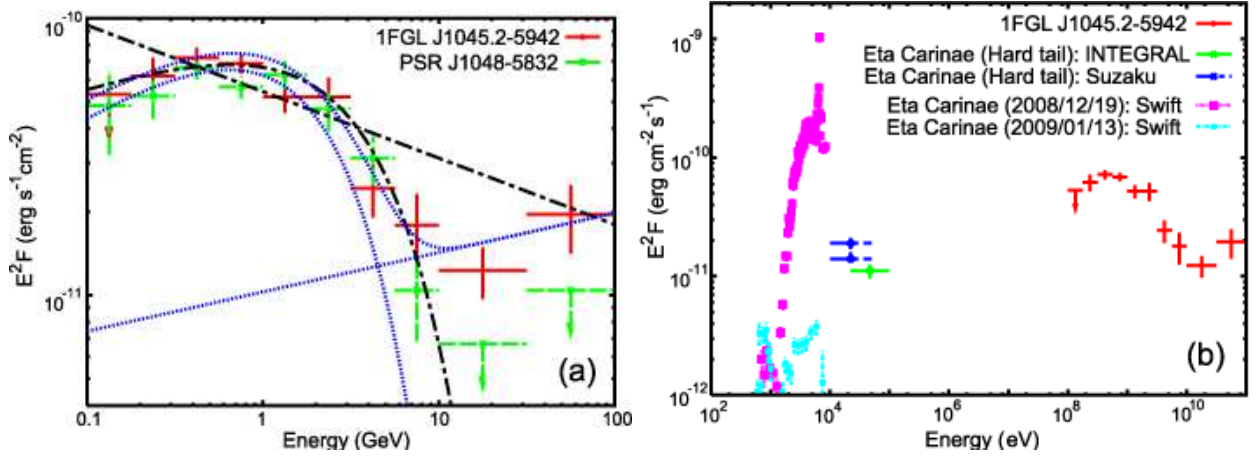


Fig. 2.— (a) Spectral energy distributions of 1FGL J1045.2–5942 (red solid points) and PSR J1048–5832 (green dashed points). The spectral points were obtained by performing likelihood analysis, assuming a single PL shape in each energy bin. The errors include both statistics and systematics. Compared to the single PL modeling for 0.1–100 GeV or the single CPL fitting for 0.1–10 GeV (black dot-dashed lines), the CPL+PL combination model (each component and their sum; blue dotted lines) represents the 0.1–100 GeV spectrum of 1FGL J1045.2–5942 best. (b) The same spectrum as (a) but with X-ray data points of η Car. While the optically-thin thermal spectra below 10 keV by the *Swift* XRT were observed during the last periastron passage simultaneously with *Fermi*, the *INTEGRAL* and *Suzaku* observations sensitive to the hard tail emission were carried out before the *Fermi* launch (Leyder et al. 2008; Sekiguchi et al. 2009).

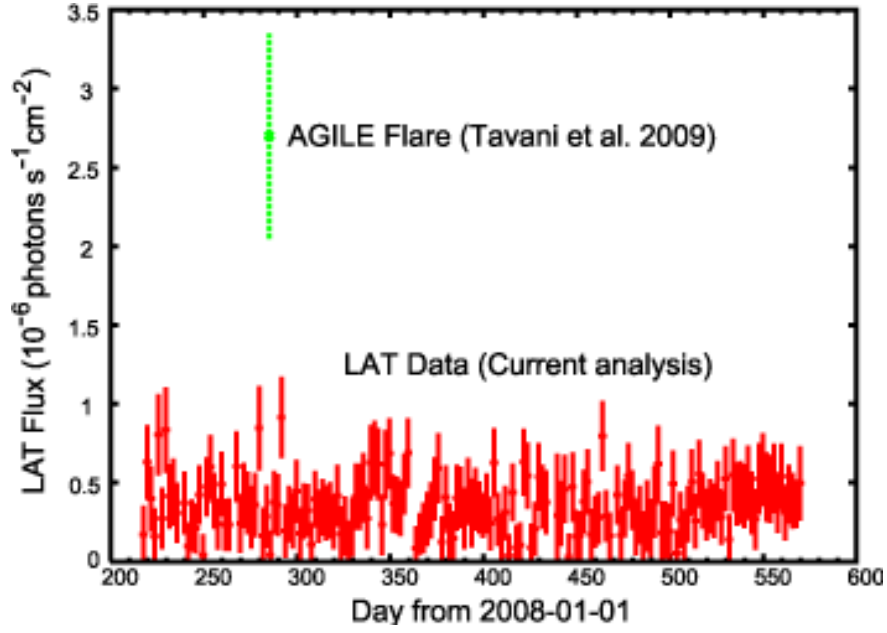


Fig. 3.— Light curve of 1FGL J1045.2–5942 by aperture photometry with the binning of 2 days. Contribution of Galactic and extragalactic diffuse emission is already subtracted. Periastron passage of η Car is around the day 360 measured from 2008 January 1st. We also show the γ -ray flux reported by Tavani et al. (2009) at day 285.

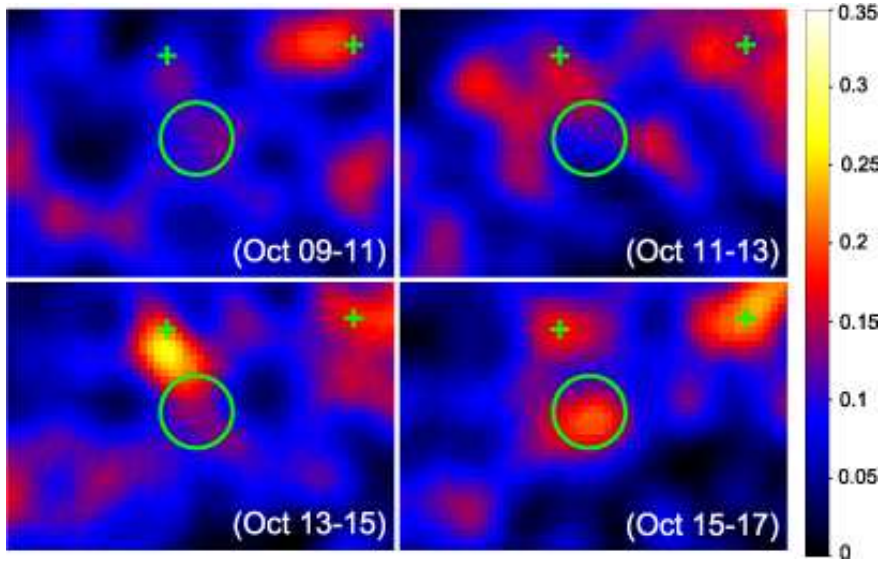


Fig. 4.— The same as the 0.1–10 GeV counts map shown in Figure 1 but for the time around the large flare reported by *AGILE* during 2008 October 11–13, corresponding to Fig. 2 of Tavani et al. (2009). Each counts map includes all of the events in the 0.1–100 GeV band with 6-bin Gaussian smoothing. The time interval in the panel labeled “Oct 11-13” is exactly the same as that of the *AGILE* flare from 2008 October 11th 02:27 to 13th 04:16 (UT), while the time intervals in the remaining panels amount to 2 days. The variation of the features among the different panels is primarily explained by statistical fluctuations due to the limited photon statistics in these short time intervals. The green circle represents the $0^\circ.5$ radius region around 1FGL J1045.2–5942, within which the LAT light curve in Figure 3 is derived. The two crosses indicate the positions of the two pulsars PSR J1048–5832 and PSR J1028–5819.

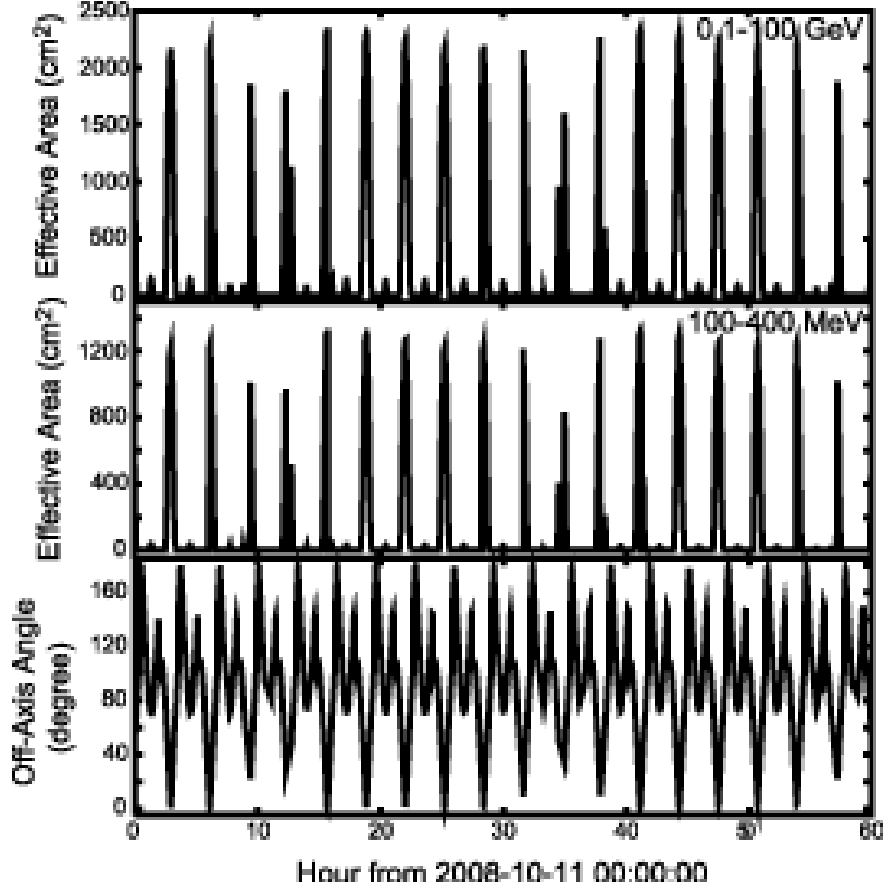


Fig. 5.— Effective area of 1FGL J1045.2–5942 in 0.1–100 GeV and 100–400 MeV energy bands by the LAT during the *AGILE* large flare. Off-axis angle from the LAT boresight to the source is also plotted at the bottom. The time binning of each plot is 60 s. According to the survey operational mode, the LAT periodically observed 1FGL J1045.2–5942 twice with the duration of ~ 50 and 20 minutes every 3 hours. See the text for more details.

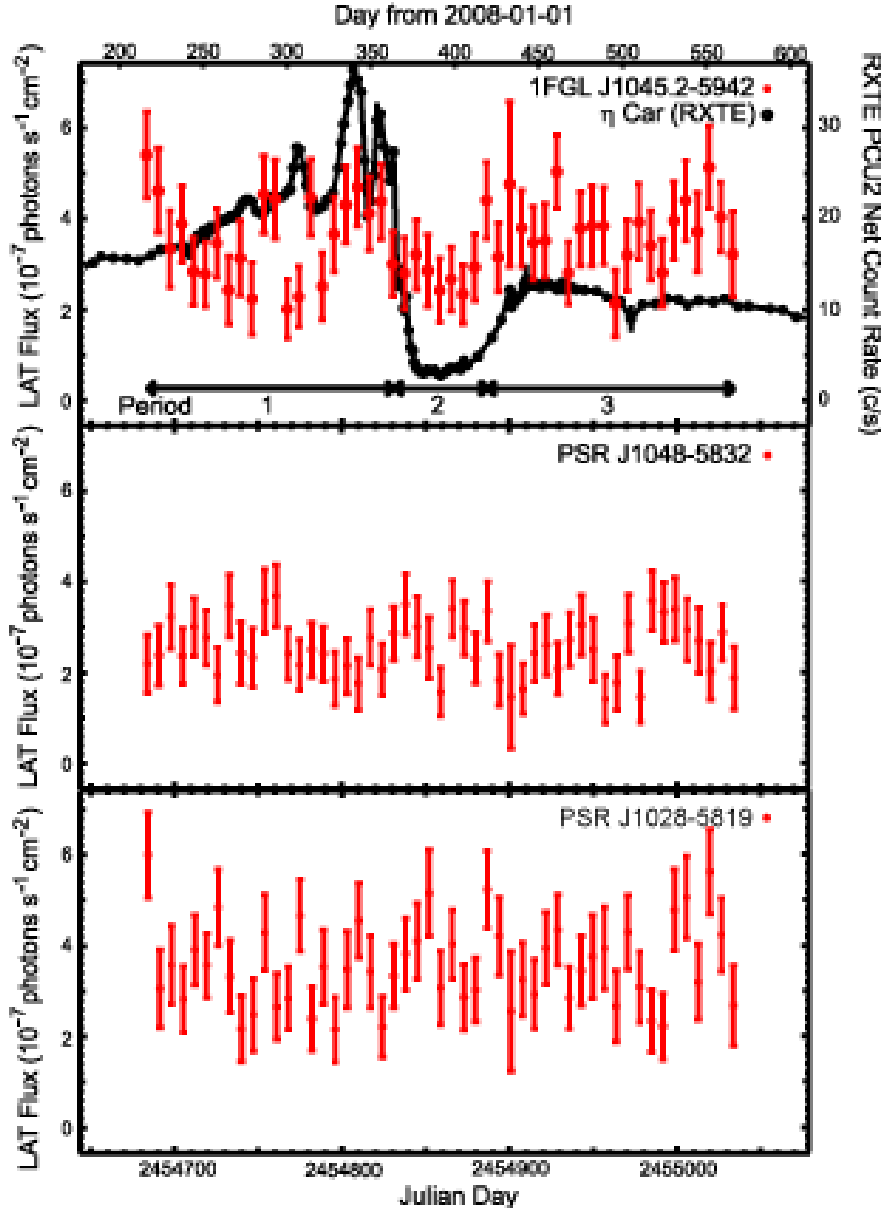


Fig. 6.— Light curves of 1FGL J1045.2–5942, PSR J1048–5832 and PSR J1028–5819 obtained by likelihood analysis. Each bin is one-week long, and the flux is in the 0.1–10 GeV energy band. The 2–10 keV X-ray light curve of η Car measured by the *RXTE* PCA is shown overlaid in the top panel (Corcoran 2009).

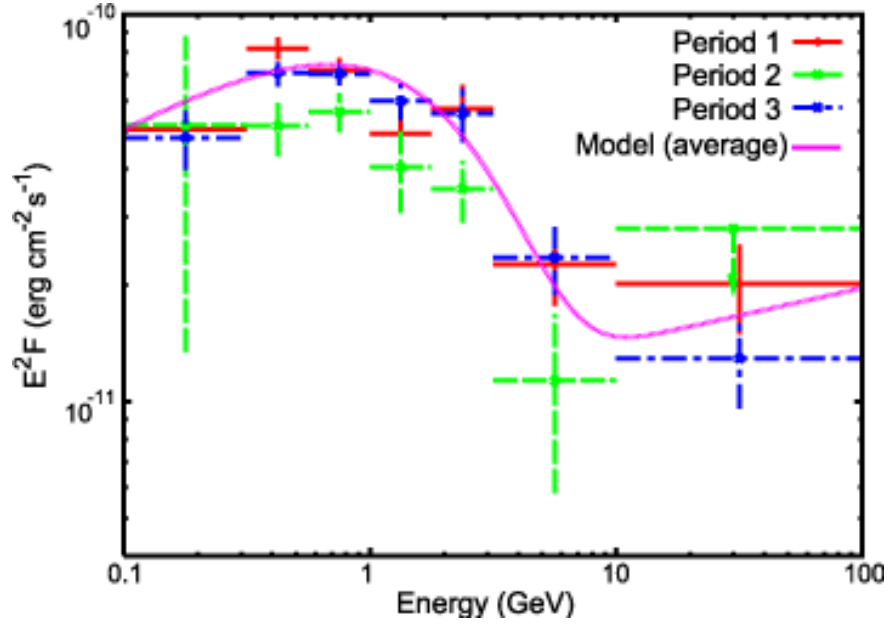


Fig. 7.— The same as Figure 2 (a) but for that of each Period in Figure 6. The best-fit model for the average spectrum is also shown (solid line).

Table 1: Spectral fitting results of the average spectrum of 1FGL J1045.2–5942 in the 0.1–100 GeV energy band.^a

Model	Photon index	Cutoff (GeV)	Photon flux (> 100 MeV) (10^{-7} photons s^{-1} cm^{-2})	TS value ^b
PL	2.2 ± 0.1	...	$4.6^{+0.5}_{-0.3}$...
CPL	2.1 ± 0.1	> 13	$4.4^{+0.2}_{-0.1}$	4
CPL+PL	1.6 ± 0.2	$1.6^{+0.8}_{-0.5}$	$3.2^{+0.3}_{-0.5}$	
	$1.9^{+0.2}_{-0.3}$...	$0.5^{+0.9}_{-0.3}$	68

^a All errors are statistical only. Systematic errors should be additionally taken into account with 10%, 5% and 20% at 100 MeV, 560 MeV and 10 GeV, respectively.

^b The TS value relative to the PL model fitting.

Table 2: The number of γ -ray events detected around the position of 1FGL J1045.2–5942 by the LAT in two selection cases (100–400 MeV in a 2° radius, and 0.1–100 GeV in $0^\circ.5$) around the date of the *AGILE* flare (October 11–13).^a

Date	100–400 MeV & 2° ^b	0.1–100 GeV & $0^\circ.5$
October 09–11	34	9
October 11–13	44	8
October 13–15	42	10
October 15–17	46	13

^a Events include the contribution from both source and diffuse background (Galactic and extragalactic) emission.

^b There are also contributions from PSR J1048–5832 and PSR J1028–5819 within the radius of 2° .

Table 3: Physical parameters of the CPL model obtained for the average and each Period spectra of 1FGL J1045.2–5942 in the 0.1–10 GeV band.^a

Period	Photon index	Cutoff (GeV)	Photon flux (> 100 MeV) (10^{-7} photons s^{-1} cm^{-2})	Energy flux (0.1–10 GeV) (10^{-10} ergs s^{-1} cm^{-2})
Average	1.8 ± 0.1	$3.3^{+1.5}_{-0.7}$	$3.7^{+0.3}_{-0.1}$	2.4 ± 0.1
1	$1.8^{+0.1}_{-0.2}$	$3.3^{+2.2}_{-1.1}$	$3.9^{+0.2}_{-0.3}$	2.5 ± 0.1
2	$1.9^{+0.2}_{-0.3}$	$3.3^{+6}_{-1.6}$	$3.4^{+0.3}_{-0.4}$	2.0 ± 0.1
3	1.8 ± 0.2	$3.5^{+3.0}_{-1.1}$	$3.9^{+0.4}_{-0.2}$	2.6 ± 0.1

^a All errors are statistical only. Systematic errors should be additionally taken into account with 10%, 5% and 20% at 100 MeV, 560 MeV and 10 GeV, respectively.